

# Passive parasitic UWB antenna capable of switched beam-forming in the WLAN frequency band using an optimal reactance load algorithm

Jung-Nam Lee  | Yong-Ho Lee | Kwang-Chun Lee | Tae Joong Kim

Hyper-connected Communication Research Laboratory, Electronics and Telecommunications Research Institute, Daejeon, Rep. of Korea

## Correspondence

Jung-Nam Lee, Hyper-connected Communication Research Laboratory, Electronics and Telecommunications Research.  
Email: jnlee77@etri.re.kr

## Funding information

This work was supported by the Institute for Information & Communications Technology Promotion (IITP) grant funded by the Korea government (MSIT) (No. 2019-0-00218, Speciality Laboratory for Wireless Backhaul Communications based on Very High Frequency).

We propose a switched beam-forming antenna that satisfies not only ultra-wideband characteristics but also beam-forming in the WLAN frequency band using an ultra-wideband antenna and passive parasitic elements applying a broadband optimal reactance load algorithm. We design a power and phase estimation function and an error correction function by re-analyzing and normalizing all the components of the parasitic array using control system engineering. The proposed antenna is compared with an antenna with a pin diode and reactance load value, respectively. The pin diode is located between the passive parasitic elements and ground plane. An antenna beam can be formed in eight directions according to the pin diode ON (reflector)/OFF (director) state. The antenna with a reactance load value achieves a better VSWR and gain than the antenna with a pin diode. We confirm that a beam is formed in eight directions owing to the RF switch operation, and the measured peak gain is 7 dBi at 2.45 GHz and 10 dBi at 5.8 GHz.

## KEYWORDS

passive parasitic element, reactance load algorithm, switched beam-forming, ultra-wideband

## 1 | INTRODUCTION

An important task of future mobile radio communication systems is to transmit more data by using limited radio resources in an efficient manner. For the development of the mobile communication technology, the frequency used increases and the number of antennas correspondingly increases based on the commercial frequency applied. However, this currently has certain disadvantages, such as high cost, high complexity, and deterioration of the antenna performance owing to the large number of antennas used for each commercial frequency band. In addition, it is impossible to mount a large number of antennas on a limited mobile terminal. Although ultra-wideband (UWB)

antennas [1–7] can cover all areas by using an omnidirectional pattern, there is a disadvantage in increasing the transmission and reception speed and capacity because the antenna gain is low. Reference [2] achieved wideband characteristics from 3 GHz to 5 GHz despite being a compact UWB antenna with a  $10 \times 10 \text{ mm}^2$  chip size. However, the maximum antenna gain was as low as 3.5 dBi and did not satisfy the WLAN frequency band. Reference [3] improved the isolation between two feeds using two fork-like stubs and implemented UWB characteristics from 2.3 GHz to 12.5 GHz using a coplanar waveguide CPW-fed microstrip antenna. However, a dual feed was used for two applications (UWB and Bluetooth), the maximum gain was 6 dBi, and beam-forming was impossible. To solve

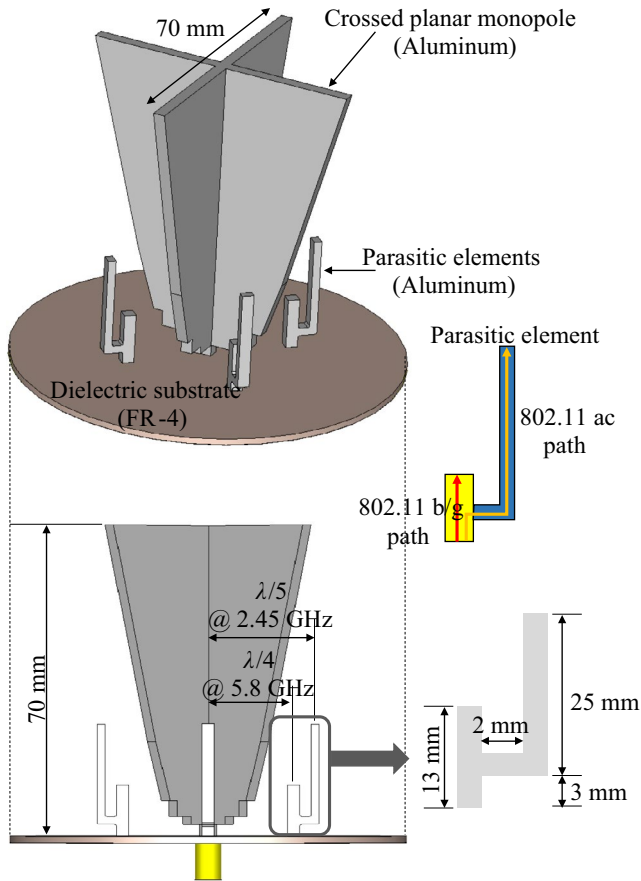


**FIGURE 1** Structure of the UWB crossed planar monopole antenna applying passive parasitic elements

the above problems, smart antenna technologies such as a phased array beam-forming antenna [8–12] and digital beam-forming antenna [13–18] capable of steering a beam in the desired direction are being studied. Conventional beam-forming antennas are effective in increasing the antenna gain using an array antenna structure. However, their use is limited owing to the use of multipole antenna elements, a narrow bandwidth, expensive phase shifters and attenuators, the increased complexity, and the overall system size. To cover the commercial frequency band and increase the gain of the desired frequency band, it is necessary to develop a small single antenna technology [19–22] that combines a UWB antenna with the beam-forming circuit technology.

In this paper, we propose a switched beam-forming antenna that not only satisfies ultra-wideband characteristics but also beam-forming within the WLAN frequency band using a UWB antenna and passive parasitic elements (PEs) applying a broadband optimal reactance load circuit. Two planar metal monopole antennas are crossed orthogonally to obtain the UWB band, and dual-band passive PEs operating at the WLAN frequency are placed around the active monopole antenna. The passive PEs are arranged in the

intersecting space generated by the crossing of the metal monopole antennas to minimize the influence of each coupling. We conduct two experiments for the beam-forming operation. First, a pin diode is attached to a passive PE to confirm the beam-forming operation characteristics. Second, we confirm the beam-forming operation characteristics by attaching the optimal beam-forming reactance load value to the passive PE. The experimental results for both cases are presented in Section 4. As the measurement results show, an eight-directional beam pattern is formed. The frequency bandwidth is from 0.8 GHz to 9 GHz, and the peak gain is 7 dBi at 2.45 GHz and 10 dBi at 5.8 GHz. We develop a switched beam-forming antenna that combines a UWB antenna, passive PEs, and broadband beam-forming reactance load matching algorithm to achieve reduction in the complexity, miniaturization, low power, and low cost.

## 2 | UWB ANTENNA DESIGN APPLYING PASSIVE PARASITIC ELEMENTS

Conventional dipole and monopole antenna technologies cannot satisfy wideband characteristics because they are antennas for narrowband characteristics. A UWB antenna should be designed to induce the flow of the current to the radiator to be as smooth as possible and to avoid sudden changes in the impedance.

Figure 1 shows the proposed UWB crossed planar metal monopole antenna with passive PEs. Two stages of the matching step were added to the bottom of the planar metal monopole for broadband matching. To smoothly induce the current flow, a modified trapezoid type radiator was designed. The passive PEs are located at a distance of  $\lambda/4$  at 5.8 GHz and  $\lambda/5$  at 2.45 GHz from the active monopole antenna. The two passive PEs are combined into one structure to operate at a dual-band frequency (2.45 GHz and 5.8 GHz). The vertically formed PEs operate at 5.8 GHz, and the bent PEs operate at 2.45 GHz. A dielectric substrate (FR-4,  $\epsilon_r$  of 4.5, and thickness of 1.6 mm) is used for attaching the reactance load circuit and fixed role of the active monopole antenna (aluminum) and passive PEs (aluminum). The lengths of the passive PEs are 13 mm and 30 mm, which are the  $\lambda/4$  values at 5.8 GHz and 2.45 GHz, respectively. The diameter of the ground plane is 80 mm, which is equivalent to  $\lambda_g/2$  at 900 MHz.

When passive PEs are placed around an active antenna, the overall antenna matching characteristics are deteriorated owing to their coupling effect. As a result, the voltage standing wave ratio (VSWR) characteristic deteriorates and the antenna gain decreases. To solve this problem, the distance between the active antenna and a passive PE is spaced at  $\lambda/2$  of the operating frequency, which causes a disadvantage in that the total antenna

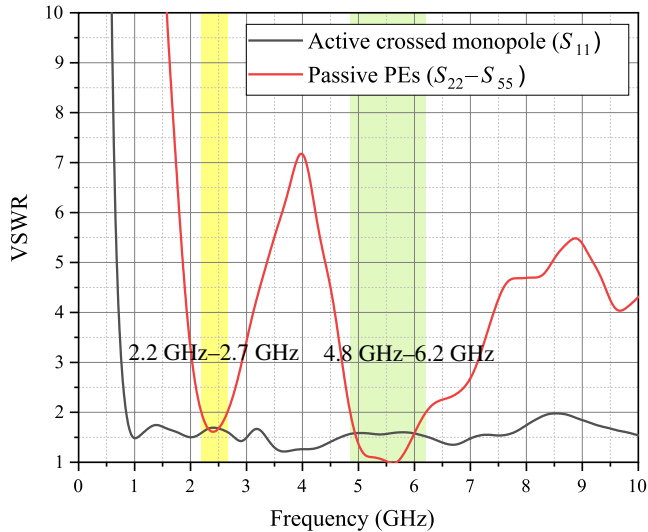


**FIGURE 2** Simulated VSWR results of the active monopole antenna and passive PEs

size increases. To minimize the change in the antenna matching characteristics owing to the influence of the passive PEs, it is necessary to add a matching circuit using lumped elements or find a suitable position of for the passive PEs that can induce optimum mutual coupling. The method of adding a matching circuit causes the manufacturing cost and complexity to increase because the lumped elements should be attached to the active antenna and passive PEs. The proposed antenna uses a method of arranging passive PEs in a space generated using crossed planar monopole antennas. The shapes of the 2.45-GHz and 5.8-GHz passive PEs are designed to be perpendicular to minimize the coupling amount while reducing the distance between the active planar monopole antenna and passive PEs.

To verify the operation of the passive PEs, we connected an SMA connector to the bottom of each passive PE to confirm that the dual-band characteristic was satisfied. Figure 2 shows the simulated VSWR results of the active crossed planar monopole antenna and passive PEs. As shown in the figure, although the passive PEs are located in the active planar

crossed monopole antenna, it ( $S_{11}$ ) satisfies the ultra-wide-band characteristics of more than 10 GHz from 0.898 GHz (VSWR < 2). The passive PEs ( $S_{22}$ – $S_{55}$ ) satisfy the dual-band characteristics from 2.2 GHz to 2.7 GHz and 4.8 GHz to 6.2 GHz (VSWR < 2).

### 3 | BROADBAND REACTANCE LOAD SEARCH ALGORITHM

To design the optimal reactance load for beam-forming, it is necessary to be able to describe mathematically the relationship between an active antenna and the passive PEs [23–26]. The optimal reactance load design is achieved by defining and evaluating the cost function based on the calculated formulas. The number of passive PEs is most dominant in describing the relationship between an active antenna and passive PEs. Assuming that the mutual coupling is very weak, it can be calculated by assuming that the PE is vacuum; however, this approach is limited because basically all the PEs are placed close to the active element in the parasitic array structure. If the number of PEs is reduced or the distance between the active element and PEs is increased, the analysis and formulation are relatively easy, but the pattern reconfigurability is lowered and various types of radiation patterns cannot be re-configured. In contrast, if additional PEs are added to improve the reconfigurability, the analysis complexity increases non-linearly, and the difficulty in impedance matching increases.

To overcome this problem, we design a power and phase estimation function and an error correction function by re-analyzing and normalizing all the components of the parasitic array using control system engineering. To reduce the complexity, the simplified power and phase estimation process is compensated using the iterations of an error correction block to calculate the approximated value as the actual value. Based on the basic concept of the function, it is possible to estimate the incident wave, reflected wave, gain estimation, weight of the embedded radiation pattern, and active-port VSWR in the parasitic array without the use of formulas. Even if the PEs increase, it is possible to easily obtain a load value very similar to the formula-based value through iterative operation processing using the function shown in Figure 3 without using a formula. Pattern modeling, described through most of this paper, mainly uses an array factor. Instead of being simple to model and analyze, this approach differs considerably from an actual radiation pattern. In this study, the radiation pattern should be formed according to the intention of the designer, which means that the error between the designed pattern shape and actual radiation pattern should be small. To reduce the modeling error, the embedded radiation pattern inherent in the antenna structure is applied to radiation pattern modeling. As the number of PEs increases, the complexity of the analysis increases and calculation of the formulas becomes difficult.

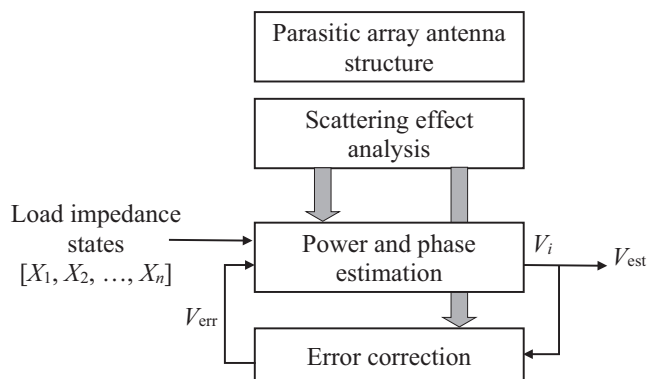
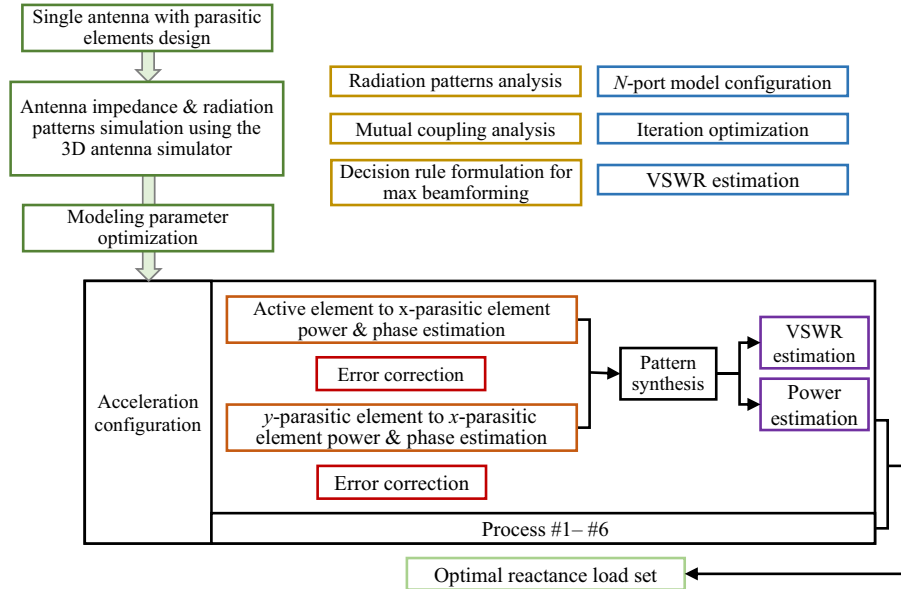
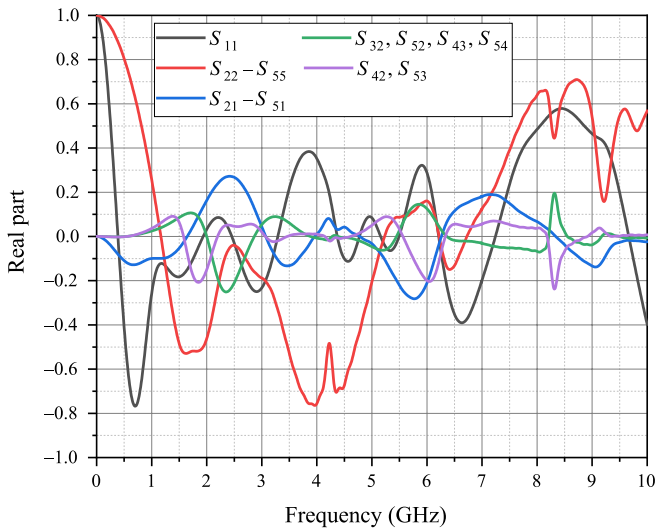


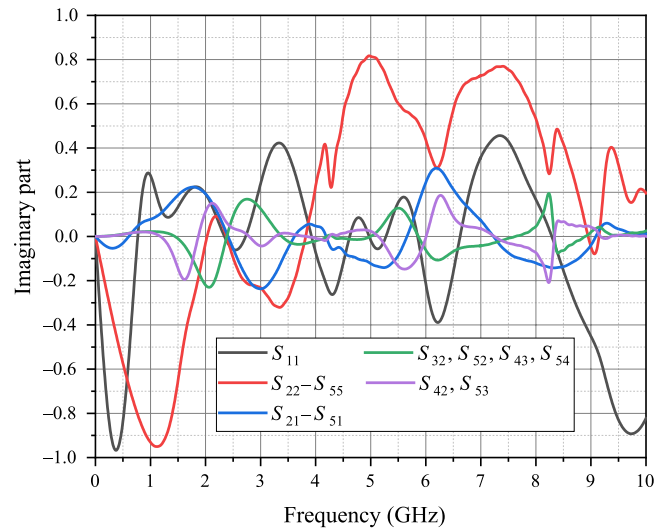
**FIGURE 3** Low-complexity antenna structure analysis method for the arrangement of multiple parasitic elements



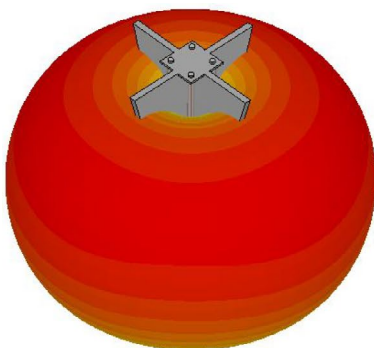
(A)



(B)



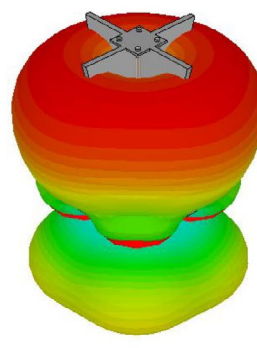
(C)



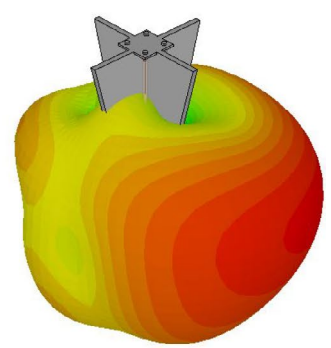
(D)



(E)



(F)



(G)

**FIGURE 4** Algorithm-based beam-forming load design: (A) Simulator configuration, (B) real part, (C) imaginary part, (D) 2.45 GHz radiation pattern at active crossed monopole, (E) 2.45 GHz radiation pattern at PE-1, (F) 5.8 GHz radiation pattern at active crossed monopole, and (G) 5.8 GHz radiation pattern at PE-1

For the reason, we proposed a method to supplement modeling using pattern data. To model a radiation pattern using an embedded radiation pattern, the virtual power source for each PE, which varies with the load impedance state of the parasitic array, should be modeled. The radiation pattern modeling of the parasitic array is designed using the analysis method shown in Figure 3. Because of the method shown in Figure 3, the beam-forming pattern design domain is transformed into a three-dimensional coordinate system, such as a spherical coordinate system in the existing domain. Based on the modeling shown in Figure 3, a beam-forming reactance load search simulator is designed, as shown in Figure 4. To calculate the optimal reactance load value, we connect an SMA connector to each passive PE as well as to the active crossed planar monopole antenna. The simulated real/imaginary impedance (Figure 4B and 4C) and radiation patterns (Figure 4D–G) at each port (port 1–port 5) were the input parameters to the beam-forming load search simulator. The input parameters were subjected to the modeling optimization process; the VSWR estimation and power evaluation were repeated; and the optimal reactance load set was then extracted.

Reference [25] shows the result of calculating the optimal reactance load value for two parasitic elements. In this paper, the optimal reactance load value is calculated by modifying this calculation [25] to an equation for four-parasitic elements.

Figure 5 shows the network model of the proposed antenna. The relationship between the active crossed monopole antenna and PEs is shown in the figure. We calculate each transfer function based on the simulated real/imaginary impedance (Figure 4B and 4C). First, the antenna pattern model is calculated as follows:

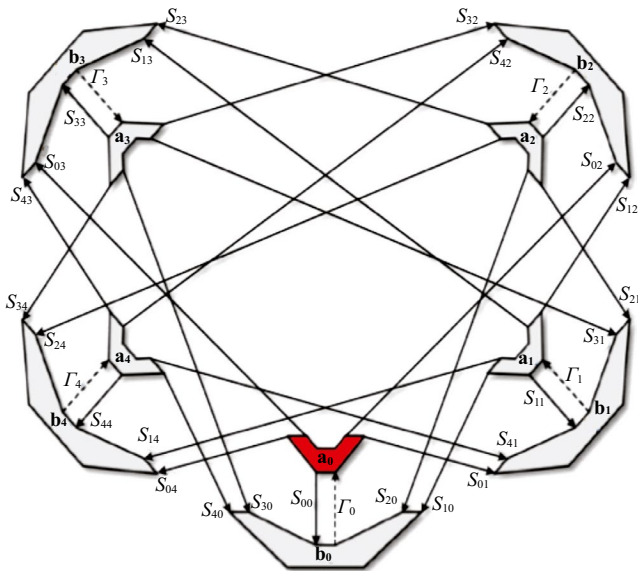


**FIGURE 5** Network model for the five-element parasitic array antenna

$$\varepsilon_{\text{unit}}(\theta, \phi) = v_{\text{inst}} \varepsilon_{\text{emb}}^T, \quad (1)$$

$$\varepsilon_{\text{emb}}^T = [\varepsilon_0(\theta, \phi) \varepsilon_1(\theta, \phi) \varepsilon_2(\theta, \phi) \varepsilon_3(\theta, \phi) \varepsilon_4(\theta, \phi)], \quad (2)$$

$$v_{\text{inst}} = [l_1 l_2 l_3 l_4], \quad (3)$$

$$l_1 = \frac{a_1}{a_0} = \Gamma_1 \frac{b_1}{a_0}, TF_{I1} [S, \Gamma_1, \Gamma_2, \Gamma_3, \Gamma_4], \quad (4)$$

$$l_2 = \frac{a_2}{a_0} = \Gamma_2 \frac{b_2}{a_0}, TF_{I2} [S, \Gamma_1, \Gamma_2, \Gamma_3, \Gamma_4], \quad (5)$$

$$l_3 = \frac{a_3}{a_0} = \Gamma_3 \frac{b_3}{a_0}, TF_{I3} [S, \Gamma_1, \Gamma_2, \Gamma_3, \Gamma_4], \quad (6)$$

$$l_4 = \frac{a_4}{a_0} = \Gamma_4 \frac{b_4}{a_0}, TF_{I4} [S, \Gamma_1, \Gamma_2, \Gamma_3, \Gamma_4]. \quad (7)$$

Here,  $S$ ,  $\Gamma_1$ ,  $\Gamma_2$ ,  $\Gamma_3$ , and  $\Gamma_4$  are mutually coupled by all the PEs. Second, we define the basic function through a radiation pattern combination based on the load impedance.

$$B_1(\theta, \phi) = \frac{\varepsilon_{\text{unit}}^{\{Z_{\text{II}}, Z_{\text{IV}}, Z_{\text{I}}, Z_{\text{III}}\}}(\theta, \phi) + \varepsilon_{\text{unit}}^{\{Z_{\text{I}}, Z_{\text{III}}, Z_{\text{II}}, Z_{\text{IV}}\}}(\theta, \phi)}{2}, \quad (8)$$

$$B_2(\theta, \phi) = \frac{\varepsilon_{\text{unit}}^{\{Z_{\text{II}}, Z_{\text{IV}}, Z_{\text{I}}, Z_{\text{III}}\}}(\theta, \phi) + \varepsilon_{\text{unit}}^{\{Z_{\text{I}}, Z_{\text{IV}}, Z_{\text{II}}, Z_{\text{III}}\}}(\theta, \phi)}{2}, \quad (9)$$

$$B_3(\theta, \phi) = \frac{\varepsilon_{\text{unit}}^{\{Z_{\text{II}}, Z_{\text{IV}}, Z_{\text{I}}, Z_{\text{III}}\}}(\theta, \phi) + \varepsilon_{\text{unit}}^{\{Z_{\text{I}}, Z_{\text{III}}, Z_{\text{I}}, Z_{\text{IV}}\}}(\theta, \phi)}{2}. \quad (10)$$

Third, we calculate the linear superposition for the embedded pattern (11) and basis functions (12).

$$\begin{aligned} \varepsilon_{\text{inst}}(\theta, \phi, s_1, s_2, s_3) &= s_{\text{in}}(s_1, s_2, s_3) \varepsilon_{\text{unit}}^{\{Z_1^{s_1, s_2, s_3}, Z_2^{s_1, s_2, s_3}, Z_3^{s_1, s_2, s_3}, Z_4^{s_1, s_2, s_3}\}}(\theta, \phi) \\ &= s_{\text{in}}(s_1, s_2, s_3) v_{\text{inst}} \varepsilon_{\text{emb}}^T, \end{aligned} \quad (11)$$

$$\varepsilon_{\text{inst}}(\theta, \phi, s_1, s_2, s_3) = s_1 B_1(\theta, \phi) + s_2 B_2(\theta, \phi) + s_3 B_3(\theta, \phi) \quad (12)$$

Fourth, we derive the reflection coefficient function per PE port based on the basis impedance, scattering parameters, and complex ratio.

$$\Gamma_1 = \frac{\frac{L_1 + L_3}{2} + S_{r1} \left( \frac{L_1 - L_3}{2} \right)}{(k_6 + k_7 (\Gamma_{\text{III}} + \Gamma_{\text{IV}}) + k_{10} \Gamma_{\text{III}} \Gamma_{\text{IV}} + \Gamma_3 (k_8 + k_9 (\Gamma_{\text{III}} + \Gamma_{\text{IV}}) + k_{11} \Gamma_{\text{III}} \Gamma_{\text{IV}}))}, \quad (13)$$

$$\Gamma_2 = \frac{\frac{L_2 + L_4}{2} + S_{r2} \left( \frac{L_2 - L_4}{2} \right)}{(k_6 + k_7 (\Gamma_1 + \Gamma_{\text{II}}) + k_{10} \Gamma_1 \Gamma_{\text{II}} + \Gamma_4 (k_8 + k_9 (\Gamma_1 + \Gamma_{\text{II}}) + k_{11} \Gamma_1 \Gamma_{\text{II}}))}, \quad (14)$$

$$\Gamma_3 = \frac{\frac{L_1+L_3}{2} + S_{r1} \left( \frac{L_3-L_1}{2} \right)}{(k_6+k_7(\Gamma_{III}+\Gamma_{IV})+k_{10}\Gamma_{III}\Gamma_{IV}+\Gamma_1(k_8+k_9(\Gamma_{III}+\Gamma_{IV})+k_{11}\Gamma_{III}\Gamma_{IV}))}, \quad (15)$$

$$\Gamma_4 = \frac{\frac{L_2+L_4}{2} + S_{r2} \left( \frac{L_4-L_2}{2} \right)}{(k_6+k_7(\Gamma_I+\Gamma_{II})+k_{10}\Gamma_I\Gamma_{II}+\Gamma_2(k_8+k_9(\Gamma_I+\Gamma_{II})+k_{11}\Gamma_I\Gamma_{II}))}. \quad (16)$$

Here,  $k_i$  and  $L_n$  are symbolic constants for all  $i$  and  $n$ .

Finally, we make a look-up table based on the calculated results. We calculate the final optimal beam-forming load set using a simulator as shown Figure 4A. As a result, the optimum beam-forming load set is  $BF_{Load} = [0.5 \text{ pF}, 3.5 \text{ nH}, 2.5 \text{ pF}, 3.5 \text{ nH}]$  (Tables 1 and 2).

## 4 | EXPERIMENT RESULTS USING PIN DIODE AND REACTANCE LOAD SET

### 4.1 | UWB passive PE antenna using PIN diode

We confirm the beam-forming characteristics by applying a pin diode to the antenna shown in Figure 1.

Figure 6 shows the pin diode circuit configuration to be attached to the passive PEs. The pin diode uses Avago's HPND-4005 and has a low capacitance value of 0.017 pF and resistance value of 4.7  $\Omega$ . The pin diode is located between the passive PEs and ground plane and has a 68-nH inductor and 47- $\Omega$  resistor for the DC block and RF choke.

**TABLE 1** Load search look-up table for proposed antenna

$S_1$	$S_2$	$S_3$	$S_{r1}$		$S_{r2}$	
			$\Gamma_1$	$\Gamma_3$	$\Gamma_2$	$\Gamma_4$
0	0	0	$Z_{II}$	$Z_I$	$Z_{IV}$	$Z_{III}$
		1	$Z_{II}$	$Z_I$	$Z_{III}$	$Z_{IV}$
		1	$Z_I$	$Z_{II}$	$Z_{IV}$	$Z_{III}$
		1	$Z_I$	$Z_{II}$	$Z_{III}$	$Z_{IV}$
1	0	0	$Z_I$	$Z_{II}$	$Z_{III}$	$Z_{IV}$
		1	$Z_I$	$Z_{II}$	$Z_{IV}$	$Z_{III}$
		1	$Z_{II}$	$Z_I$	$Z_{III}$	$Z_{IV}$
		1	$Z_{II}$	$Z_I$	$Z_{IV}$	$Z_{III}$

**TABLE 2** Optimum load sets

	Ports 2 and 3	Ports 4 and 5
Load set	$Z_I, Z_{II}$	$Z_{III}, Z_{IV}$
Calculated load set	0.5 pF, 3.5 nH	2.5 pF, 3.5 nH

When a DC voltage is applied (3 V), the pin diode turns ON and the passive PEs are connected to the ground plane, as shown in Figure 6C, and thus, the passive PEs operate as reflectors. Conversely, when the DC voltage is changed to 0 V, the passive PEs and ground plane are opened, and the passive PEs operate as directors to radiate the current in a free space. Table 3 presents the beam-forming scheme according to the pin diode operation. An antenna beam can be formed in eight directions according to the pin diode ON/OFF state.

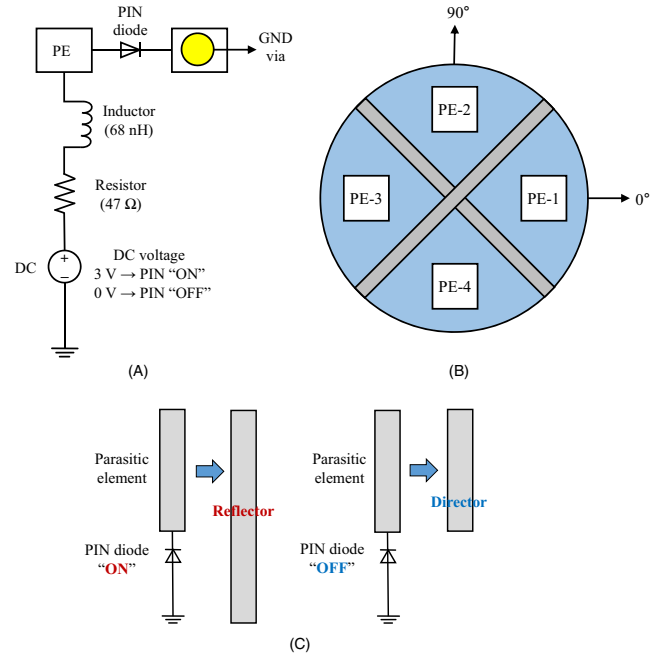


**FIGURE 6** Pin diode configuration and operation mechanism: (A) pin diode circuit modeling, (B) passive PE position (top plane), and (C) passive PE operation mechanism using the pin diode

**TABLE 3** Beam-forming mechanism of the proposed antenna using a pin diode

Beam direction	Supplied DC voltage '1' = ON and '0' = OFF			
	PE-1	PE-2	PE-3	PE-4
Mode 1				
0°	0	1	1	1
90°	1	0	1	1
180°	1	1	0	1
270°	1	1	1	0
Mode 2				
45°	0	0	1	1
135°	1	0	0	1
225°	1	1	0	0
315°	0	1	1	0

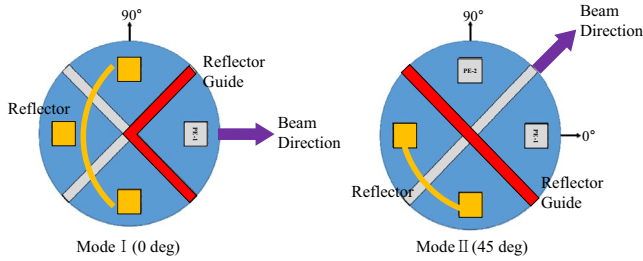


**FIGURE 7** Reflector guide operation mechanism

As shown in Figure 7, the three ON-state passive PEs operate as reflectors to push the current, and the crossed planar monopole operates as a reflector guide to further collect the antenna beam in the OFF-state passive PE direction. It is expected that the antenna gain characteristics will be further improved owing to the operation mechanism displayed in Figure 7. A parasitic beam-forming antenna using a switch or diode can cause the antenna characteristics to change depending on the mismatch between the switching element and a passive PE and the internal capacitance of the diode. The proposed antenna minimizes the mismatch by simplifying the structure of the switching circuit and minimizes the changes in the antenna characteristics by using the pin diode with minimum internal capacitance.

Figure 8 shows the VSWR measurement results according to the scheme presented in Table 3. As shown in Figure 8, the antenna characteristics do not change in all the cases, and the frequency of 0.8 GHz–6.5 GHz is satisfied at  $VSWR < 2$ . To verify the beam-forming operation characteristics, radiation patterns are measured based on the scheme given in Table 3.

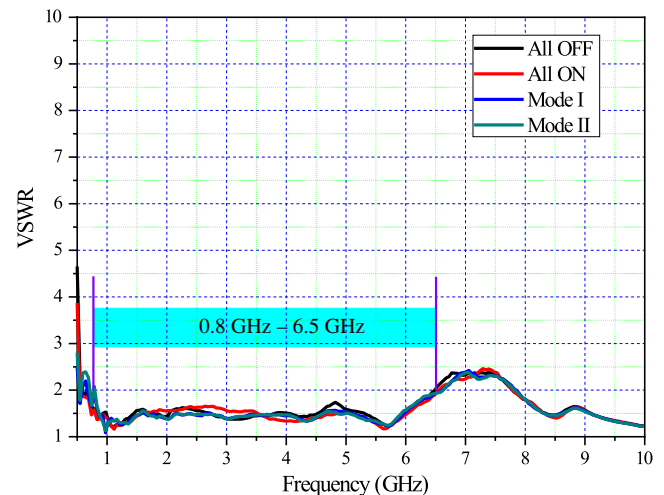
The experiment results for the radiation patterns were obtained in an anechoic chamber at the Daedeok Radio Engineering Center, Daejeon, Korea. Figure 9 shows the measured and simulated radiation patterns in modes 1 and 2. It can be confirmed that beam-forming occurs in the 2.45-GHz and 5.8-GHz WLAN frequency bands according to the ON/OFF state of the pin diode. The simulated peak gain is 5.6 dBi at 2.45 GHz and 7.8 dBi at 5.8 GHz. The measured peak gain is 6 dBi at 2.45 GHz and 8 dBi at 5.8 GHz. Although not mentioned in this paper, omnidirectional patterns were measured outside the beam-forming frequency band.

## 4.2 | UWB passive PE antenna using the optimal reactance load

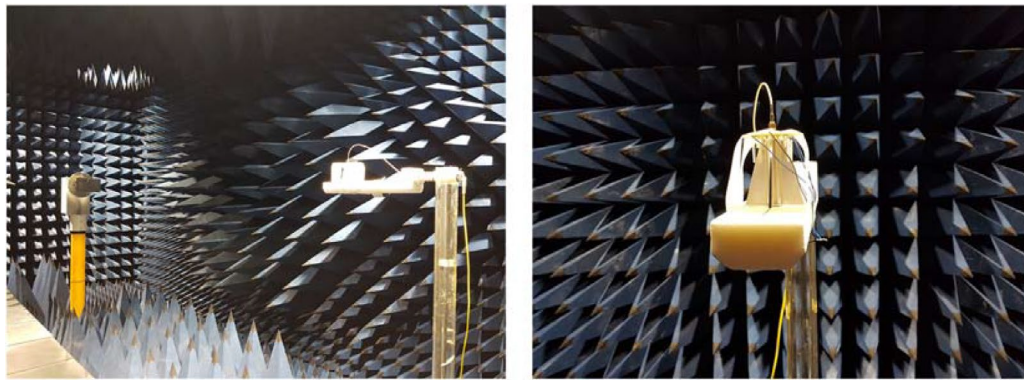
We fabricated and measured the optimum reactance load value calculated using a beam-forming reactance load simulator. The optimum beam-forming load set was  $BF_{Load} = [0.5 \text{ pF}, 3.5 \text{ nH}, 2.5 \text{ pF}, 3.5 \text{ nH}]$ .

Figure 10 shows the structure of the UWB crossed planar monopole antenna with a reactance load value. To fix the active antenna, a support top-loading plate is implemented on top of the crossed planar monopole antenna, and the active antenna is fixed by fastening four nonmetallic supporters. Passive PEs are fixed to the dielectric substrate using nonmetallic screws, and a microstrip circuit is constructed to attach the reactance load value and RF switches to the side of the passive PEs. The RF switch used is SKY13575-639LF of Skyworks [27], and the operating principle is given in Table 4. The reactance load value calculated using the beam-forming reactance load simulator is shown in Figure 10C. A DC voltage of 3 V is commonly applied to the VDD port, and beam-forming is implemented by changing the control voltage of VC1 and VC2. The RF-4 port of the RF switch is open, and the RF-4 port is responsible for the RF-2 port because there are two identical 3.5 nH inductance values at the calculated reactance load value. The simulation results using the 3D electromagnetic and beam-forming reactance simulator show that a beam is formed in the direction of 0.5 pF across the inductance value, and the RF switch configuration for the beam-forming is given in Table 5.

Figure 11 shows the results of the VSWR measurement and simulation according to the scheme in Table 5. To reduce the weight of the antenna, the active antenna and passive PEs were made of aluminum and consist of a DC voltage supply line for applying the DC voltage. The DC voltage was applied to the RF switches, and the active crossed planar monopole antenna was connected to the vector network analyzer to measure the VSWR according to the change in the control voltage. The vector network analyzer used in the measurement was a Rohde & Schwarz vector network analyzer capable of measuring up to 40 GHz. Figure 11A shows the VSWR-simulated



**FIGURE 8** VSWR measurement results of the proposed antenna using pin diode



(A)

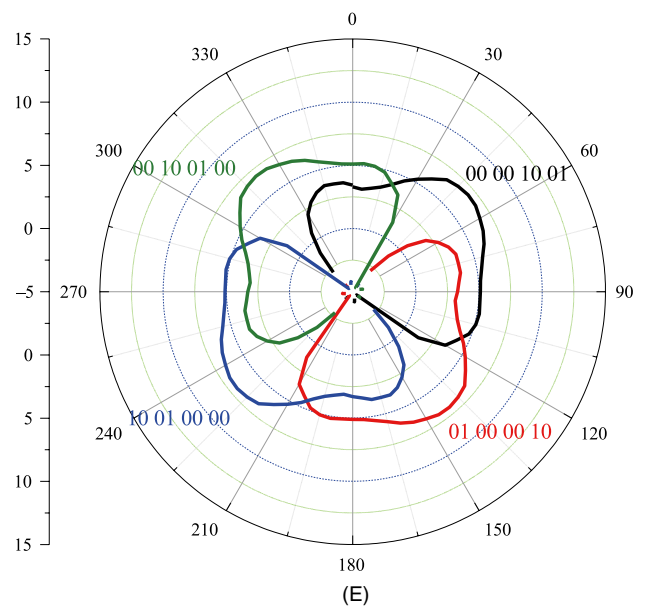
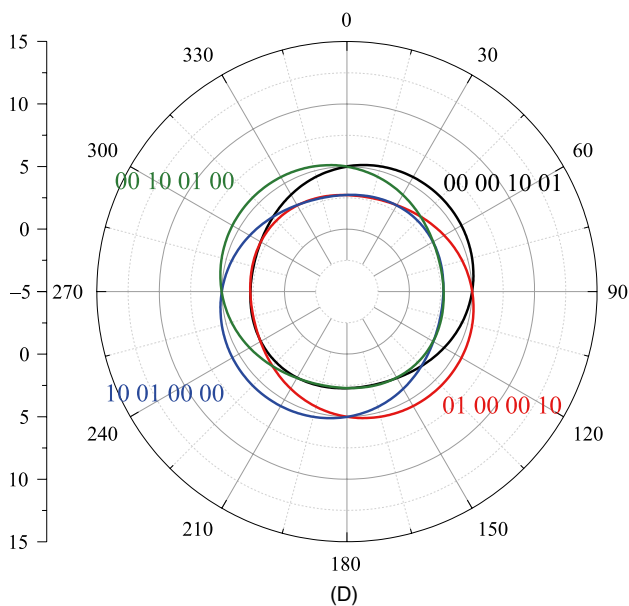
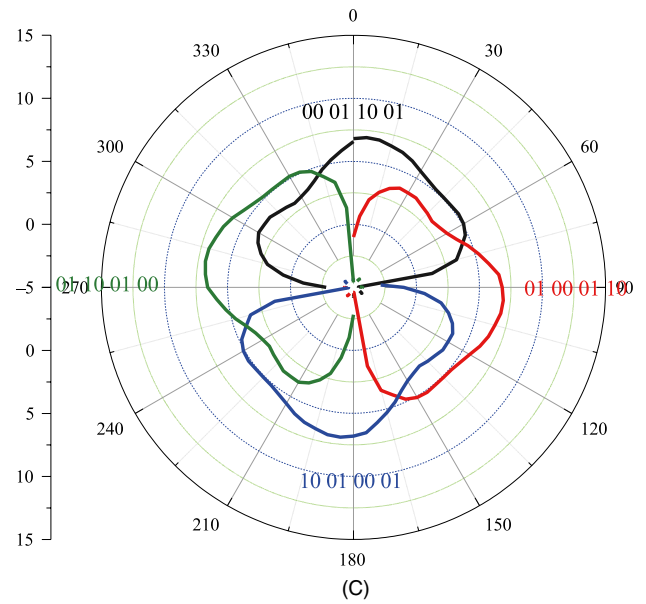
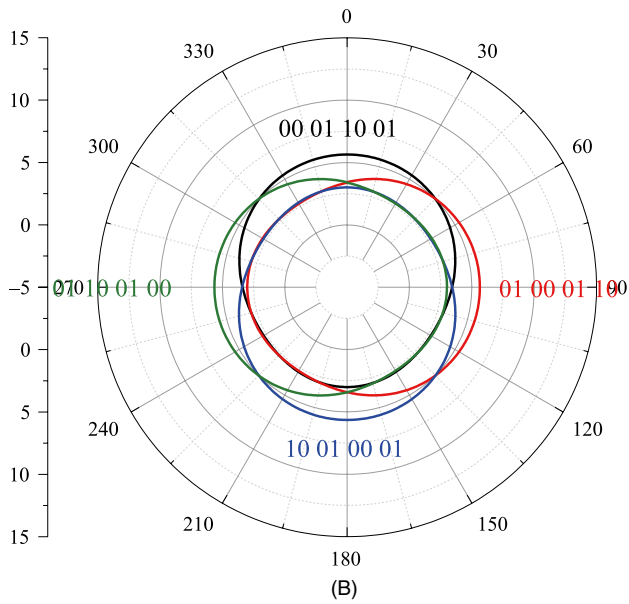


**FIGURE 9** Measured and simulated radiation patterns with a pin diode: (A) Radiation pattern measurement environment, (B) simulated pattern of mode 1 at 2.45 GHz, (C) measured pattern of mode 1 at 2.45 GHz, (D) simulated pattern of mode 2 at 2.45 GHz, (E) measured pattern of mode 2 at 2.45 GHz, (F) simulated pattern of mode 1 at 5.8 GHz, (G) measured pattern of mode 1 at 5.8 GHz, (H) simulated pattern of mode 2 at 5.8 GHz and (I) measured pattern of mode 2 at 5.8 GHz

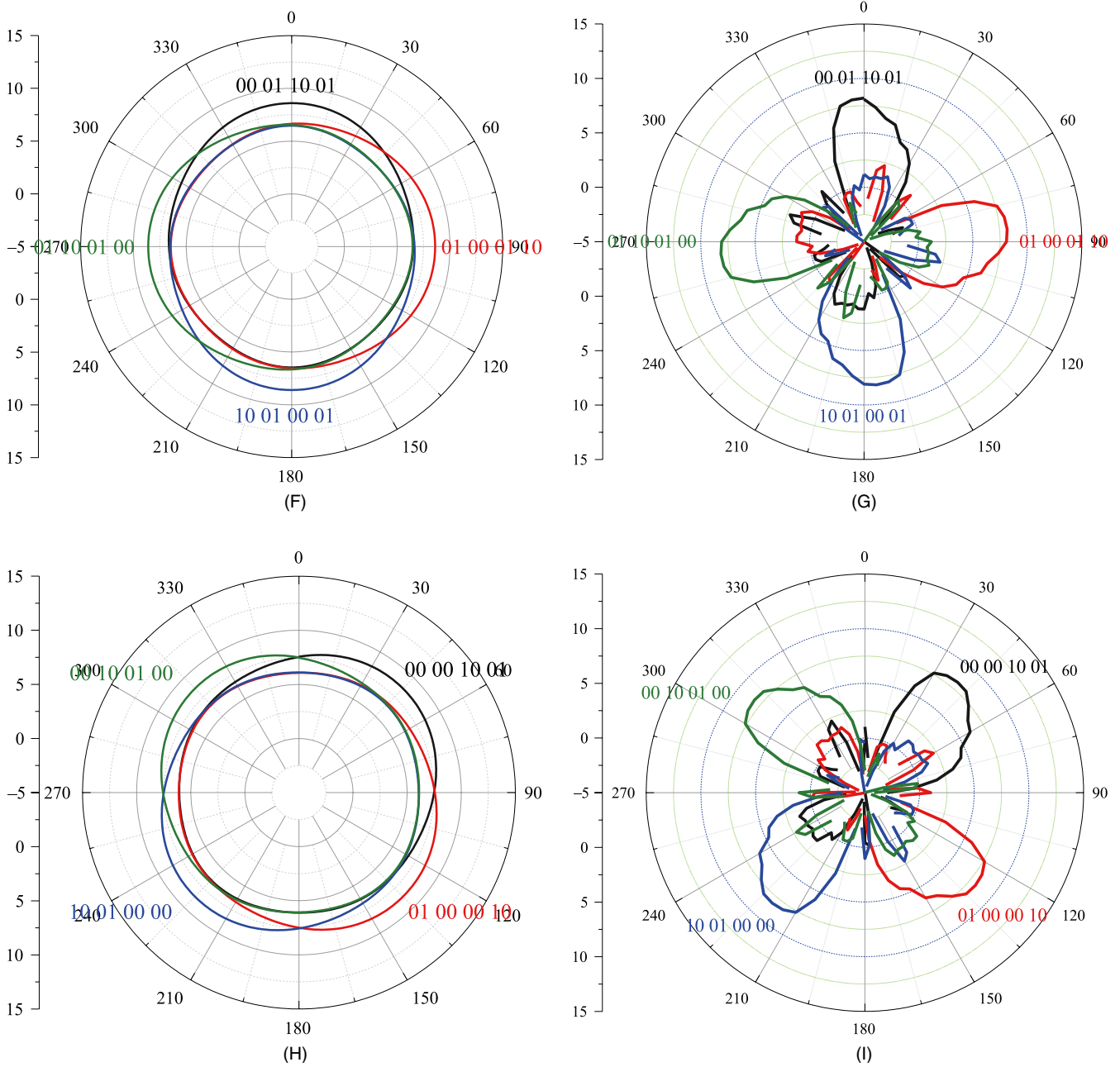
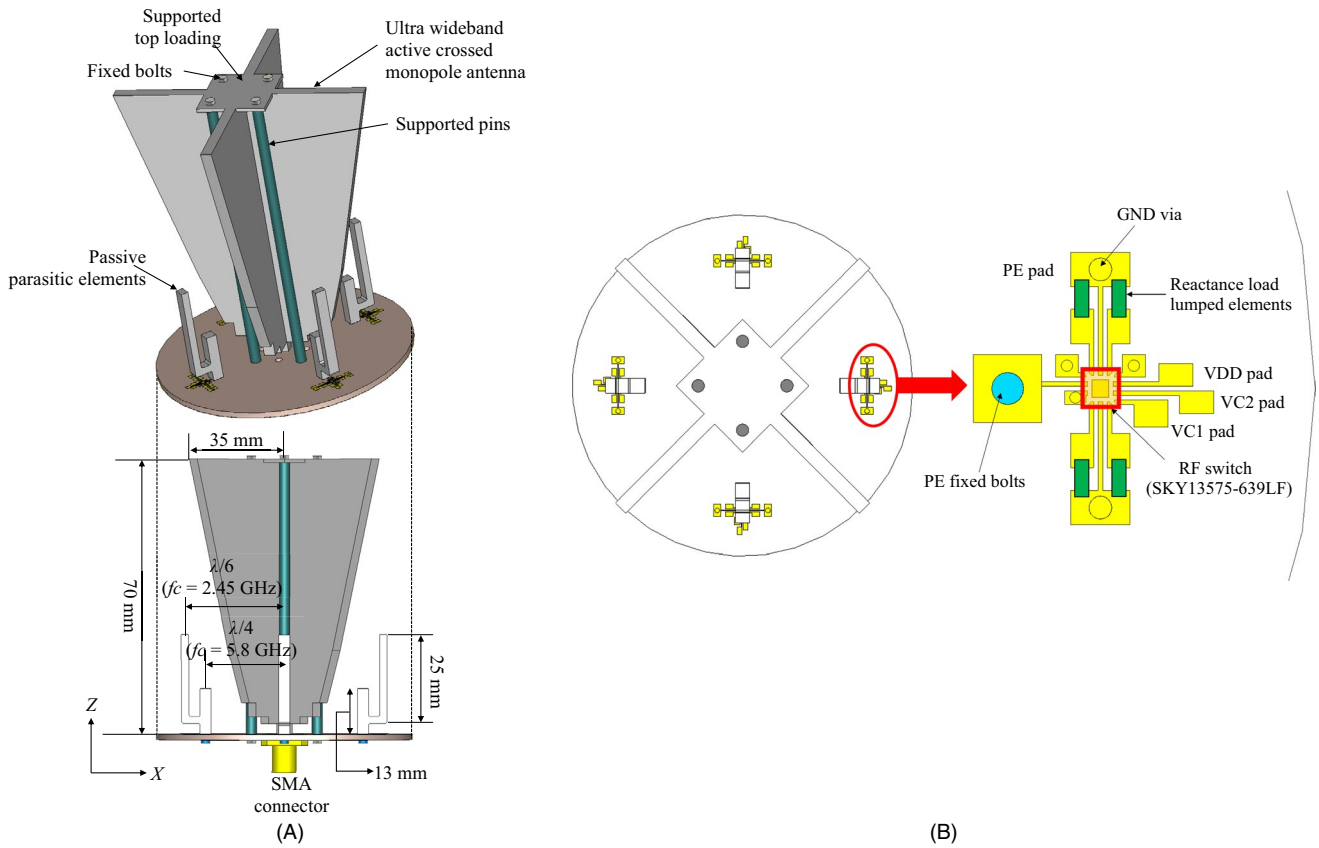


FIGURE 9 (Continued)

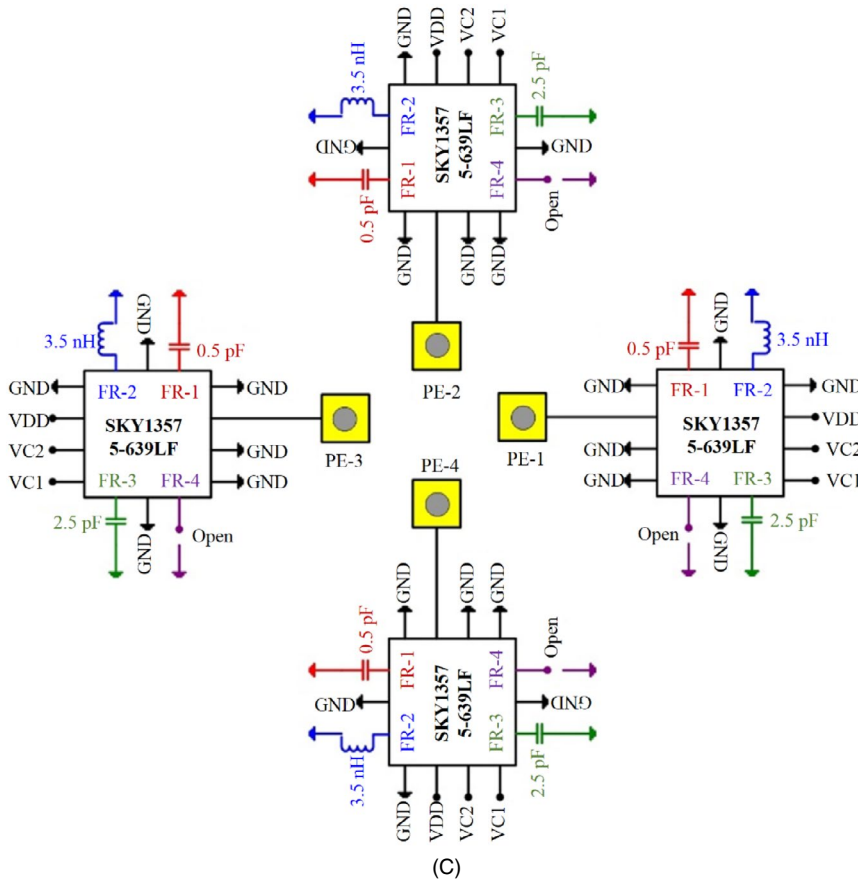
results using the electromagnetic and beam-forming reactance load simulators, which are almost the same. The simulated frequency bandwidth is 0.9 GHz–6.0 GHz (VSWR < 2). As shown in Figure 11B, the proposed antenna characteristics did not change in all the cases, and a frequency of 0.8 GHz–9.0 GHz is satisfied at VSWR < 2. To verify the beam-forming operation characteristics, the radiation patterns were measured based on the scheme shown in Table 5.

Figure 12 shows the radiation pattern simulation results in mode 1 based on Table 5 using the electromagnetic and beam-forming reactance load simulators. The results

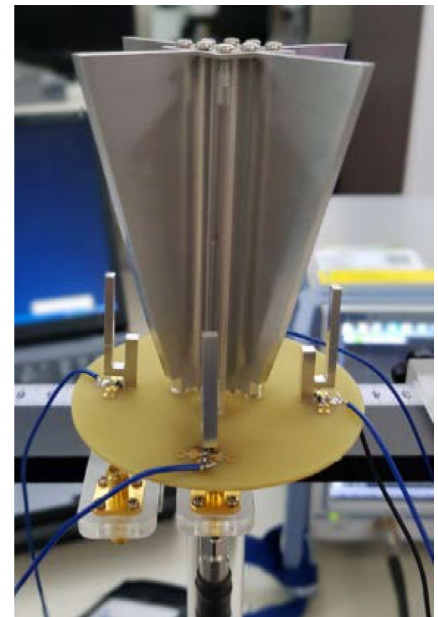
of the two simulators at 0° in mode 1 are in reasonable agreement. The pattern correlation of the two simulators is 0.99 based on the maximum value of 1. This means that it reduces the error between the algorithm-based simulator using MATLAB and electromagnetic-based 3D simulator. It is possible to reduce the antenna designing process and time by reducing the error caused by the difference in the analysis method applied by the two simulators. The simulated peak gain is 6.9 dBi at 2.45 GHz and 9.12 dBi at 5.8 GHz. The radiation pattern in mode 1 based on Table 5 is simulated using a beam-forming reactance load simulator. As shown in Figure 12, it is confirmed that the



(B)



(C)



(D)

**FIGURE 10** The proposed prototype antenna: (A) Antenna structure, (B) configuration of the RF switches, (C) beam-forming operation mechanism, and (D) prototype antenna

**TABLE 4** Switch operating principle

	VC1	VC2
RFC to RF1	0	0
RFC to RF2	0	1
RFC to RF3	1	0
RFC to RF4	1	1

beam-forming is applied according to the change in the reactance value. In the simulation, only the radiation pattern of mode 1 was considered. The simulation accuracy was confirmed by measuring the radiation pattern in an anechoic chamber.

Figure 13 shows the measured and simulated radiation patterns in modes 1 and 2 based on Table 5. It can be confirmed that beam-forming is achieved in the 2.45-GHz and 5.8-GHz WLAN frequency bands according to the reactance load value. The measured radiation patterns are tilted about 5°. It is expected to be a problem owing to the open state without attaching lumped elements to the RF-4 port of the RF switch. This problem could be solved by attaching a 3.5-nH inductor to the RF-4 port. As shown in Figure 13E, other frequencies outside the WLAN frequency are measured for omnidirectional patterns. The measured peak gain is 7 dBi at 2.45 GHz and 10 dBi at 5.8 GHz (Table 6).

## 5 | CONCLUSION

We proposed a switched beam-forming antenna that satisfies not only ultra-wideband characteristics but also

**TABLE 5** Beam-forming principle of the proposed antenna using a reactance load

Beam direction	Supplied DC voltage Control voltage '1' = 3V and '0' = 0V							
	PE-1		PE-2		PE-3		PE-4	
	VC1	VC2	VC1	VC2	VC1	VC2	VC1	VC2
Mode 1								
0°	0	0	0	1	1	0	0	1
90°	0	1	0	0	0	1	1	0
180°	1	0	0	1	0	0	0	1
270°	0	1	1	0	0	1	0	0
Mode 2								
45°	0	0	0	0	1	0	0	1
135°	0	1	0	0	0	0	1	0
225°	1	0	0	1	0	0	0	0
315°	0	0	1	0	0	1	0	0

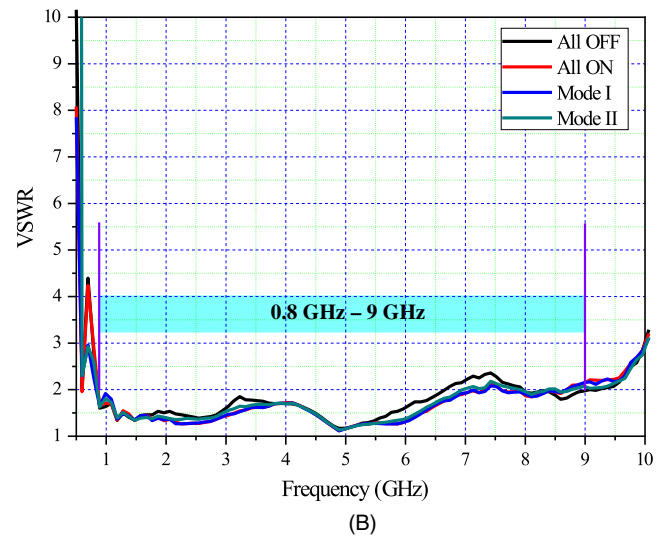
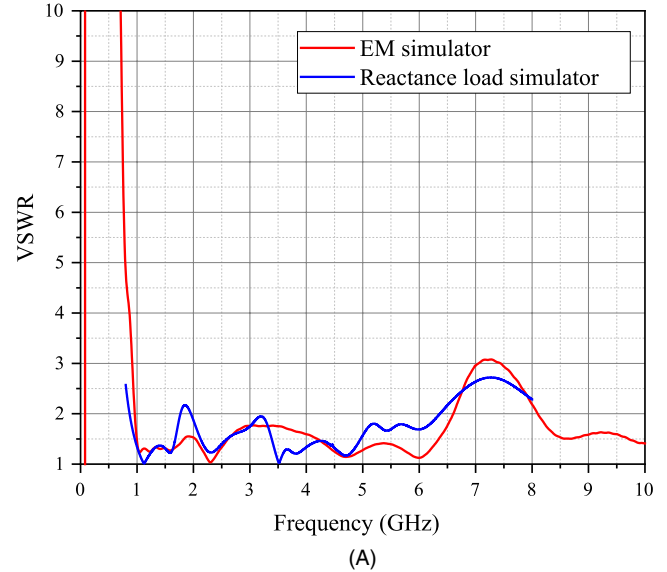
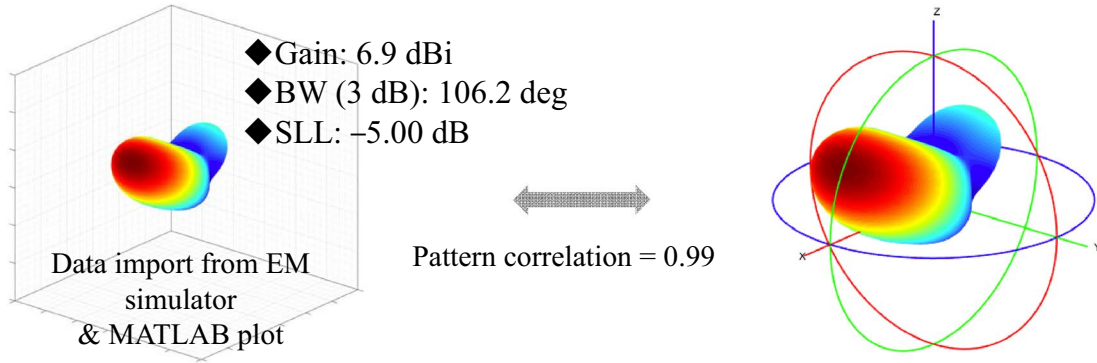
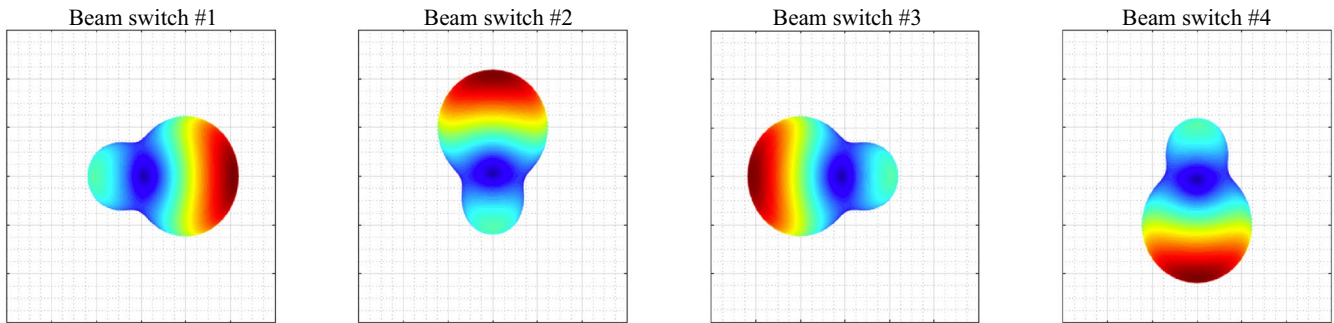


**FIGURE 11** Measured and simulated VSWR results for all the cases: (A) Simulated result and (B) measured result

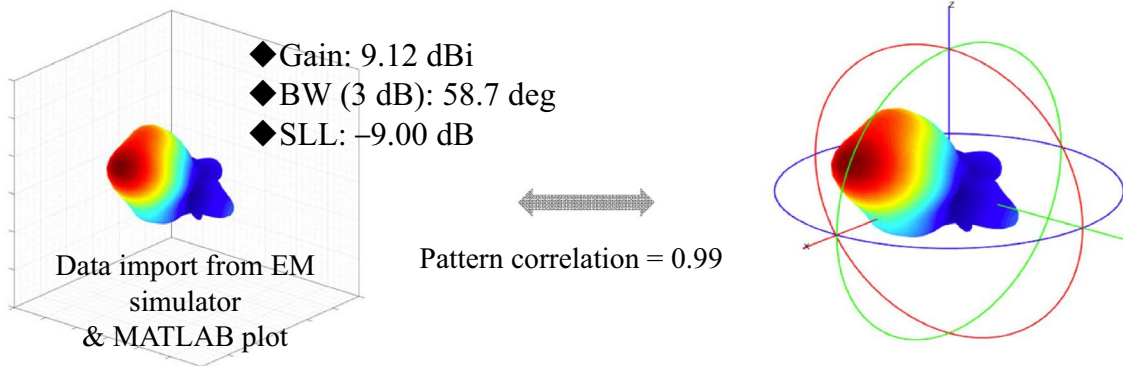


[ Total far-field EM simulation pattern]

[ Total far-field pattern synthesis (MATLAB) ]

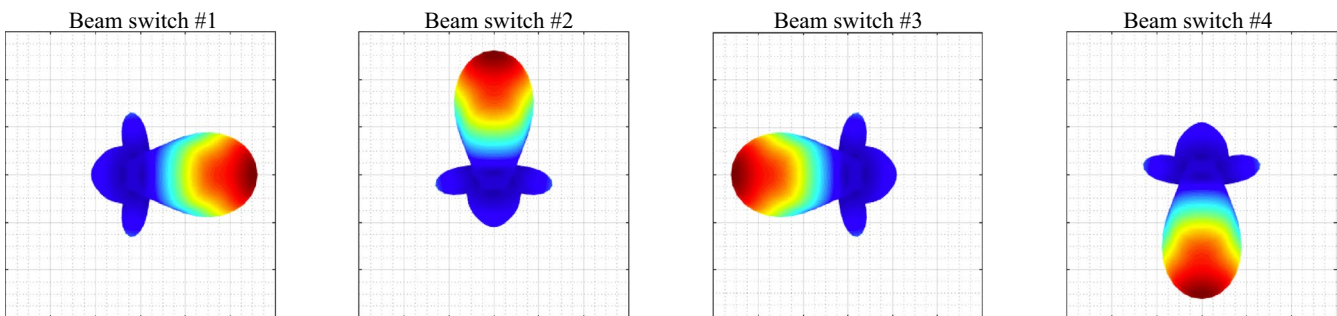


(A)



[ Total far-field EM simulation pattern]

[ Total far-field pattern synthesis (MATLAB) ]



(B)

FIGURE 12 Simulated radiation patterns with the reactance load: (A) mode 1 at 2.45 GHz and (B) mode 1 at 5.8 GHz

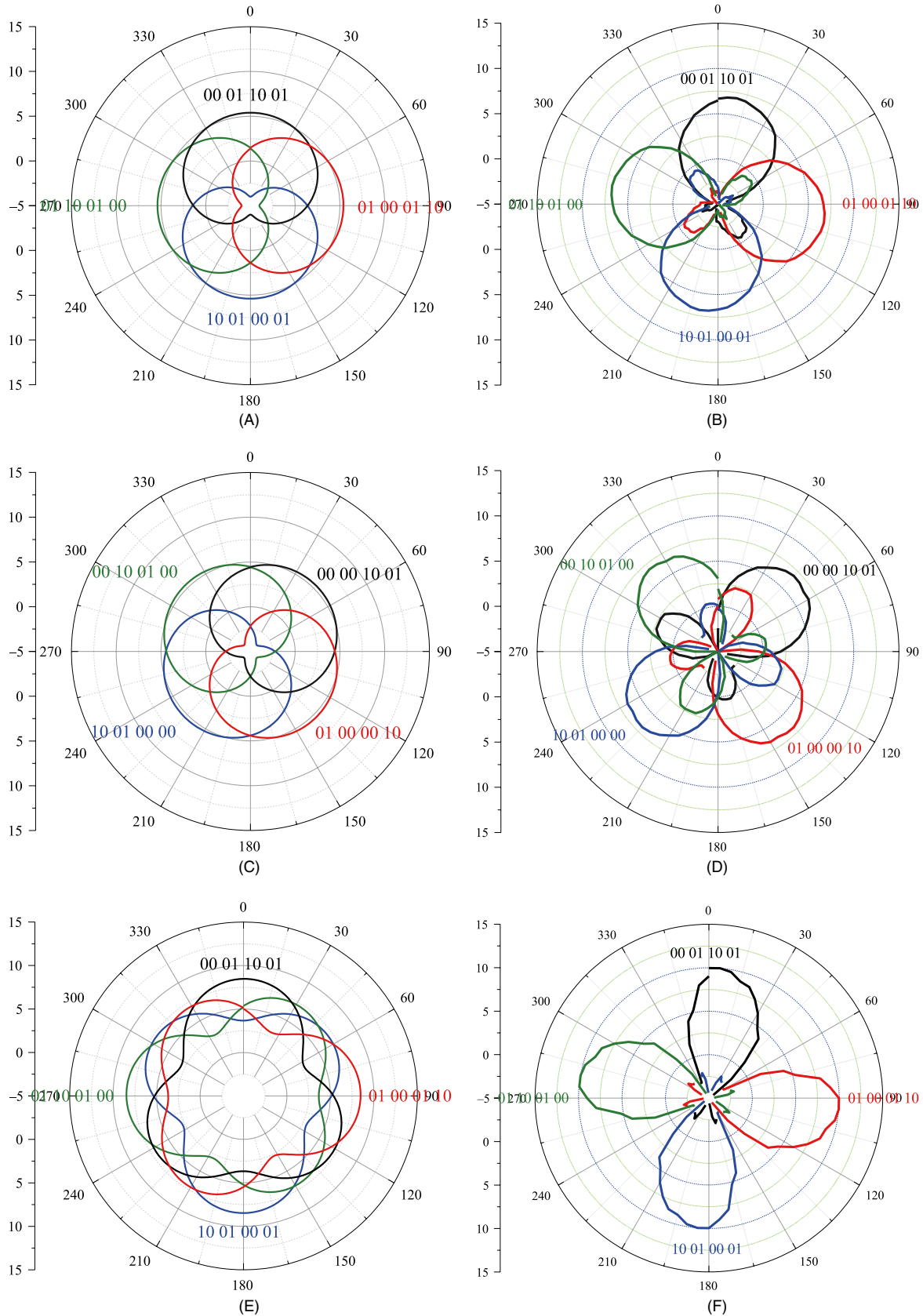


**FIGURE 13** Measured and simulated radiation patterns with the reactance load: (A) Simulated pattern of mode 1 at 2.45 GHz, (b) measured pattern of mode 1 at 2.45 GHz, (C) simulated pattern of mode 2 at 2.45 GHz, (D) measured pattern of mode 2 at 2.45 GHz, (E) simulated pattern of mode 1 at 5.8 GHz, (F) measured pattern of mode 1 at 5.8 GHz, (G) simulated pattern of mode 2 at 5.8 GHz, (H) measured pattern of mode 2 at 5.8 GHz, (I) simulated pattern at other frequencies, and (J) measured pattern at other frequencies

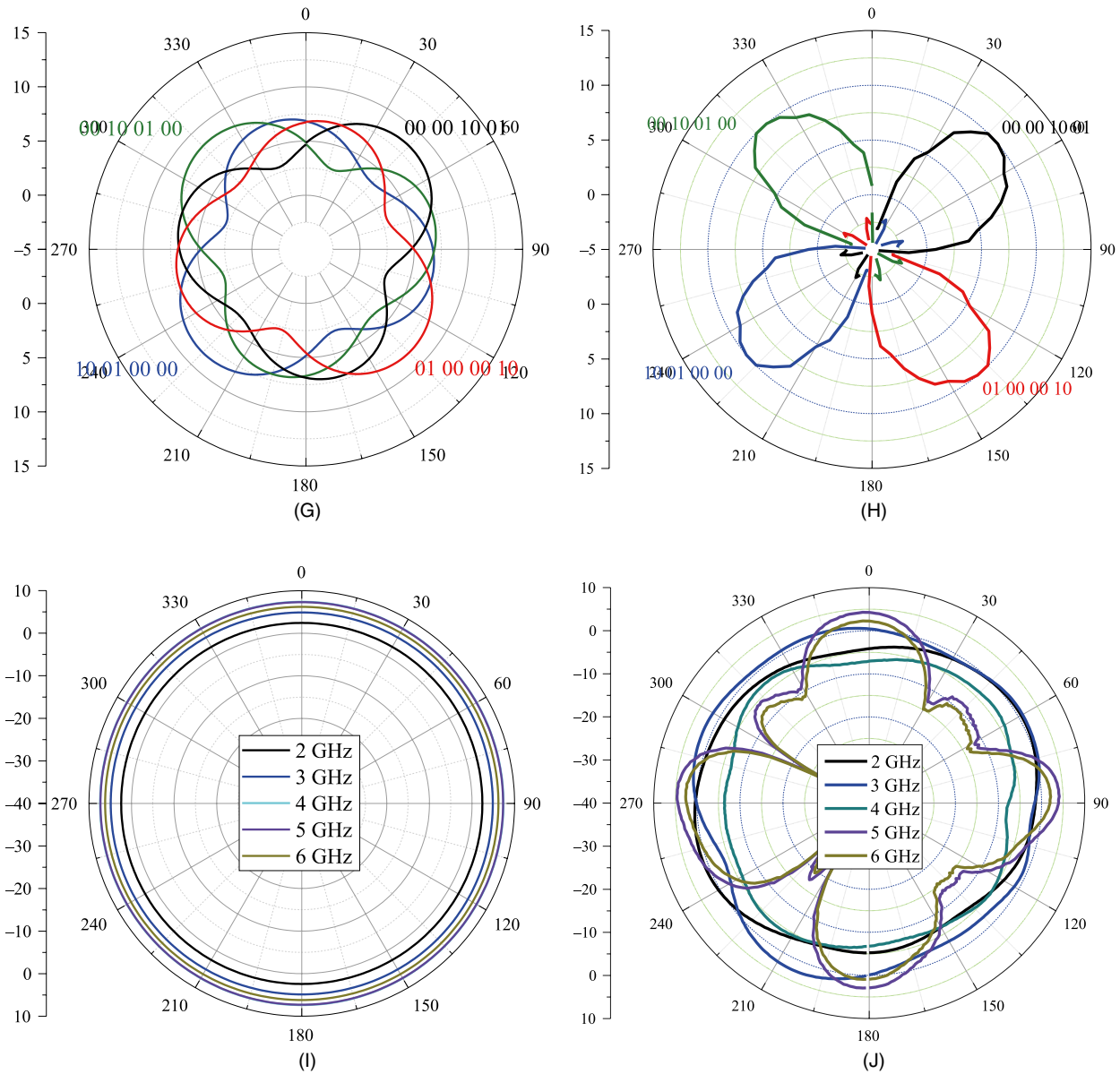


FIGURE 13 (Continued)

beam-forming in the WLAN frequency band using a UWB antenna and passive PEs applying a broadband optimal reactance load. The value of the optimum reactance load is calculated using a beam-forming load search algorithm simulator. We designed a power and phase estimation function

as well as an error correction function by reanalyzing and normalizing all the components of the parasitic array using control system engineering. By simply attaching optimum loads to the RF switch, a simple design and compact antenna structure are provided. We compared the results of the 3D

TABLE 6 Comparison of the proposed antenna characteristics

	3D simulator	Algorithm	PIN diode	Reactance load
Frequency (GHz)	0.9–6.0	0.9–6.0	0.8–6.5	0.8–9.0
Radiation pattern	Beam-forming	Beam-forming	Beam-forming	Beam-forming
Antenna gain	6.9dBi @ 2.45 GHz 9.12 dBi @ 5.8 GHz	6.9dBi @ 2.45 GHz 9.12 dBi @ 5.8 GHz	6dBi @ 2.45 GHz 8 dBi @ 5.8 GHz	7 dBi @ 2.45 GHz 10 dBi @ 5.8 GHz
Size (mm <sup>2</sup> )	50 × 70	50 × 70	50 × 70	50 × 70

and beam-forming reactance load simulator and confirmed the agreement between the two results. The proposed antenna was compared with ones with a pin diode and the reactance load value, respectively. The antenna with the reactance load value achieved a better VSWR and gain than the antenna with the pin diode. We confirmed that a beam was formed in eight directions owing to the RF switch operation, and the measured peak gain was 7 dBi at 2.45 GHz and 10 dBi at 5.8 GHz. We proposed an antenna that could achieve WLAN frequency band beam-forming without beam-forming elements while satisfying UWB frequency characteristics. The proposed antenna could be capable of beam-forming in the desired frequency band by changing the type of passive PE applied.

## ACKNOWLEDGMENTS

This work was supported by the Institute for Information & Communications Technology Promotion (IITP) grant funded by the Korea government (MSIT) (No. 2019-0-00218, Speciality Laboratory for Wireless Backhaul Communications based on Very High Frequency).

## ORCID

Jung-Nam Lee  <https://orcid.org/0000-0002-2058-5048>

## REFERENCES

- J. N. Lee et al., *Design of an ultra-wideband antenna using a ring resonator with a notch function*, ETRI J. **35** (2013), no. 6, 1075–1083.
- J. N. Lee and J. K. Park, *Compact uwb chip antenna design using the coupling concept*, Prog. Electromag. Res. **90** (2009), 341–351.
- P. Gao and S. He, *A compact uwb and bluetooth slot antenna for mimo/diversity applications*, ETRI J. **36** (2014), no. 2, 309–312.
- J. N. Lee et al., *Design of dual-band antenna with u-shaped open stub for wlan/uwb applications*, Microw. Opt. Technol. Lett. **51** (2009), no. 2, 284–289.
- J. N. Lee, J. K. Park, and I. H. Choi, *A compact filter-combined ultra-wideband antenna for uwb applications*, Microw. Opt. Technol. Lett. **50** (2008), no. 11, 2839–2845.
- J. N. Lee, J. K. Park, and S. S. Choi, *Design of a compact frequency notched uwb slot antenna*, Microw. Opt. Technol. Lett. **48** (2006), no. 1, 105–107.
- J. N. Lee and J. K. Park, *Impedance characteristics of a trapezoidal ultra-wideband antenna having a notch function*, Microw. Opt. Technol. Lett. **46** (2005), no. 5, 503–506.
- L. C. Godara, *Application of antenna arrays to mobile communications. II. Beam-forming and direction-of-arrival considerations*, Proc. IEEE. **85** (1997), no. 8, 1195–1245.
- M. V. Ivashina et al., *An optimal beamforming strategy for wide-filed surveys with phased-array-fed reflector antennas*, IEEE Trans. Antennas Propag. **59** (2011), no. 6, 1864–1875.
- X. Gao, L. Dai, and A. M. Sayeed, *Low RF-complexity technologies to enable millimeter-wave mimo with large antenna array for 5g wireless communications*, IEEE Commun. Mag. **56** (2018), no. 4, 211–217.
- K. Kibaroglu, M. Sayginer, and G. M. Rebeiz, *An Ultra low-cost 32-element 28 GHz phased-array transceiver with 41 dBm EIRP and 1.0 – 1.6 Gbps 16-QAM link at 300 meters*, in IEEE Radio Freq. Integrat. Circuits Symp. Honolulu, HI, USA, June 2017, pp. 73–76.
- S. Zhang et al., *A planar switchable 3-D-coverage phased array antenna and its user effects for 28-GHz mobile terminal applications*, IEEE Trans. Antennas Propag. **65** (2017), no. 12, 6413–6421.
- S. Han et al., *Large-scale antenna systems with hybrid analog and digital beamforming for millimeter wave 5G*, IEEE Commun. Mag. **53** (2015), no. 1, 186–194.
- J. D. Fredrick, Y. Wang, and T. Itoh, *A smart antenna receiver array using a single RF channel and digital beamforming*, IEEE Trans. Microw. Theory Tech. **50** (2002), no. 12, 3052–3058.
- W. Roh et al., *Millimeter-wave beamforming as an enabling technology for 5g cellular communications: theoretical feasibility and prototype results*, IEEE Commun. Mag. **52** (2014), no. 2, 106–113.
- J. Zhang, W. Wu, and D. G. Fang, *Single RF channel digital beamforming multibeam antenna array based on time sequence phase weighting*, IEEE Antennas Wirel. Propag. Lett. **10** (2011), 514–516.
- M. Harter et al., *24 GHz digital beamforming radar with T-shaped antenna array for three-dimensional object detection*, Int. J. Microw. Wireless Technol. **4** (2011), no. 3, 327–334.
- S. Kim and Y. E. Wang, *A series-fed microstrip receiving array for digital beamforming*, IEEE Antennas Wirel. Propag. Lett. **3** (2004), 332–335.
- D. H. Gwak, I. S. Sohn, and S. H. Lee, *Analysis of single-RF MIMO receiver with beam-switching antenna*, ETRI J. **37** (2015), 647–656.
- P. K. Pal and R. S. Sherratt, *MIMO channel capacity and configuration selection for switched parasitic antennas*, ETRI J. **40** (2018), 197–206.
- Y. K. Cho et al.,  *$\lambda/16$  spaced single RF chain MIMO antenna using low-power CMOS switches*, Eur. Microw. Conf., Paris, France, Dec. 2015, pp. 726–729.
- S. Zhang, I. Strytsin, and G. F. Pedersen, *Compact beam-steerable antenna array with two passive parasitic elements for 5G mobile terminals at 28 GHz*, IEEE Trans. Antennas Propag. **66** (2018), 5193–5203.
- M. Yousefbei and J. P. Carrier, *Towards compact and frequency-tunable antenna solutions for MIMO transmission with a single RF chain*, IEEE Trans. Antennas Propag. **62** (2014), no. 3, 1065–1073.
- J. Cheng, Y. Kamiya, and T. Ohira, *Adaptive beamforming of ESPAR antenna based on steepest gradient algorithm*, IEICE Trans. Commun. **E84-B** (2001), no. 7, 1790–1800.
- C. Sun et al., *Fast beamforming of electronically steerable parasitic array radiator antenna: Theory and experiment*, IEEE Trans. Antennas Propag. **52** (2004), no. 7, 1819–1832.
- M. Yousefbei, O. N. Alrabadi, and J. P. Carrier, *Efficient MIMO transmission of PSK signals with a single-radio reconfigurable antenna*, IEEE Trans. Commun. **62** (2014), 567–577.
- SKY13575-639LF Datasheet and Product Info, <http://www.skyworksinc.com>.

## AUTHOR BIOGRAPHIES



**Jung-Nam Lee** received his BS and MS degrees from the Department of Information and Communication Engineering, Hanbat National University, Daejeon, Rep. of Korea, in 2004 and 2006, respectively. He received his PhD degree in Radio Wave Engineering from Hanbat National University in 2010. Since 2011, he is with the Electronics and Telecommunications Research Institute, Daejeon, Rep. of Korea, where he is currently a senior researcher. His research interests include small antennas, millimeter wave antennas, terahertz antennas, RFID antennas, UWB antennas, beam-forming antennas, and small base station antenna design.



**Yong-Ho Lee** received his MS degree from the University of Science and Technology, Daejeon, Rep. of Korea in 2009. Since 2009, he is with the Electronics and Telecommunications Research Institute, Daejeon, Rep. of Korea, where he is currently a senior researcher. His research interests include wireless communication, single-RF MIMO, beam-forming, and 5G physical layer design.



**Kwang-Chun Lee** received his BS/MS degree in electronic engineering from Chungang University, Seoul, Rep. of Korea in 1986 and 1988, respectively. He received his PhD in Information and Communication Engineering from Chungbuk National University, Korea in 2013. Since 1988, he is with the Electronics and Telecommunications Research Institute. His primary research interests include beam-forming antennas and RF technologies for mobile communication system design.



**Tae Joong Kim** received his BS, MS, and PhD degrees from Yonsei University, Seoul, Rep. of Korea in 1991, 1993, and 1998, respectively. From 1998 to 2000, he was a senior researcher at the Electronics and Telecommunications Research Institute, Daejeon, Rep. of Korea. He joined Eonex Ltd. in 2001, where he initially worked in chipset system design and subsequently in software protocol stack and field tests until 2006. He returned to the Electronics and Telecommunications Research Institute in 2006 and developed 4G-LTE and 5G mobile communication systems. He is currently the Assistant Vice President of the Future Mobile Communication Research Division at the Electronics and Telecommunications Research Institute and is involved in managing projects sponsored by the government for technology beyond 5G.